

**$B \rightarrow X_s \gamma \gamma$  and  $B_s \rightarrow \gamma \gamma$  in supersymmetry with broken R-parity**Alexander Geminert,<sup>\*</sup> Shaouly Bar-Shalom,<sup>†</sup> and Gad Eilam<sup>‡</sup>*Technion-Israel Institute of Technology,  
32000 Haifa, Israel*

(Dated: February 1, 2008)

We examine the effects of R-parity violating (RPV) supersymmetry on the two-photon B decays  $B \rightarrow X_s \gamma \gamma$  and  $B_s \rightarrow \gamma \gamma$ . We find that, although there are many one-loop RPV diagrams that can contribute to these two-photon B decays, the RPV effect is dominated by a single diagram. This diagram, named here  $\lambda$ -irreducible, has a distinct topology which is irrelevant for the  $b \rightarrow s \gamma$  amplitude at one-loop and has thus a negligible effect on the one-photon decay  $B \rightarrow X_s \gamma$ . We show that the  $\lambda$ -irreducible RPV diagram can give  $BR(B_s \rightarrow \gamma \gamma) \sim 5 \times 10^{-6}$  and  $BR(B \rightarrow X_s \gamma \gamma) \sim 6 \times 10^{-7}$ , which is about 16 and 5 times larger than the SM values, respectively. Although the enhancement to the decay width of  $B \rightarrow X_s \gamma \gamma$  is not that dramatic, we find that the energy distribution of the two photons is appreciably different from the SM, due to new threshold effects caused by the distinct topology of the RPV  $\lambda$ -irreducible diagram. Moreover, this diagram significantly changes the forward-backward asymmetry with respect to the softer photon in  $B \rightarrow X_s \gamma \gamma$ . Thus, the RPV effect in  $B \rightarrow X_s \gamma \gamma$  can be discerned using these observables.

PACS numbers:

**I. INTRODUCTION**

Supersymmetry (SUSY) is considered to be one of the most promising candidates for new physics, curing some of the shortcomings of the Standard Model (SM), for instance, the emergence of quadratic divergences in the Higgs sector [1]. However, despite its appealing theoretical features, so far there is no direct experimental evidence for SUSY up to the electroweak scale. Apart from direct production and decays of SUSY particles, indirect probes could be employed to search for SUSY in processes where the SUSY particles emerge virtually either in loops or as tree-level mediators. In this respect, Flavor Changing Neutral Current (FCNC) or Lepton Flavor Violating (LFV) processes are a natural search ground for SUSY, since the SM contribution to such processes is either loop-suppressed (FCNC) or it is essentially absent (LFV).

If R-parity ( $R_p$ ) is violated in the SUSY superpotential, then such flavor changing transitions can emerge from interactions of squarks or sleptons with fermions. R-parity is defined by  $R_p \equiv (-1)^{3(B-L)+2s}$ , where  $B$  stands for baryon number,  $L$  for lepton number, and  $s$  is the spin of the particle. Thus,  $R_p = 1$  for all particles, while  $R_p = -1$  for sparticles. The RPV terms in the superpotential that we will employ are:

$$W_{RPV} = \frac{1}{2} \lambda_{ijk} \epsilon_{ab} \hat{L}_i^a \hat{L}_j^b \hat{E}_k^c + \lambda'_{ijk} \epsilon_{ab} \hat{L}_i^a \hat{Q}_j^b \hat{D}_k^c, \quad (1)$$

where  $\hat{Q}$  and  $\hat{L}$  are SU(2) doublet quark and lepton supermultiplet, respectively, and  $\hat{D}^c$  and  $\hat{E}^c$  denote the SU(2) singlet down-type quark and lepton supermultiplet, respectively. Also,  $i, j, k$  are generation indices and  $\lambda_{ijk} = -\lambda_{jik}$  due to the antisymmetric SU(2) indices  $a, b$ . The above RPV operators may lead to some drastic changes in SUSY phenomenology. For example, the lightest sparticle becomes unstable and decays to SM particles and single particles may be produced in collider experiments.

In this paper we examine the effects of the RPV SUSY sector on the two-photon  $b \rightarrow s$  transition amplitude  $b \rightarrow s \gamma \gamma$ , focusing on the two decay channels  $B_s \rightarrow \gamma \gamma$  and  $B \rightarrow X_s \gamma \gamma$ . These two processes have received considerable attention in the past decade or so [2, 3, 4, 5, 6, 7, 8, 9, 10]. Let us denote by  $BR^M(B \rightarrow X_s \gamma \gamma)$  and  $BR^M(B_s \rightarrow \gamma \gamma)$  the branching ratios calculated within a given model  $M$ . In the SM, the one-loop ElectroWeak (EW) diagrams give [4, 5] (see also the next sections):  $BR^{SM}(B \rightarrow X_s \gamma \gamma) \sim BR^{SM}(B_s \rightarrow \gamma \gamma) \sim 10^{-7}$ . The leading order QCD corrections to these decays can increase the SM branching ratios by more than 100% [6, 8].

The effects of physics beyond the SM on the  $b \rightarrow s \gamma \gamma$  amplitude have also been considered. In the 2-Higgs Doublet Model (2HDM) the  $BR(B \rightarrow X_s \gamma \gamma)$  can range from  $0.1 \times BR^{SM}(B \rightarrow X_s \gamma \gamma)$  to  $10 \times BR^{SM}(B \rightarrow X_s \gamma \gamma)$  [5, 8] and in a four generation model  $BR(B_s \rightarrow \gamma \gamma) \sim 10 \times BR^{SM}(B_s \rightarrow \gamma \gamma)$  [9]. In addition, the  $b \rightarrow s \gamma \gamma$  transition amplitude was investigated within R-parity conserving (RPC) SUSY in [7], where only a subset of the RPC SUSY one-loop diagrams was included (i.e., diagrams with charged Higgs and chargino exchanges, neglecting possible flavor changing

<sup>\*</sup>phcga@physics.technion.ac.il<sup>†</sup>shaouly@physics.technion.ac.il<sup>‡</sup>eilam@physics.technion.ac.il

neutralino and gluino exchanges). With these assumptions, [7] found that,  $BR^{RPC}(B_s \rightarrow \gamma\gamma)$  is highly correlated to  $BR^{RPC}(B \rightarrow X_s\gamma)$  and is, therefore, bound to be within  $\pm 30\%$  of the SM prediction, due to the constraints from the measured value of  $BR(B \rightarrow X_s\gamma)$ .

The purpose of this work is to estimate only the effects of the RPV sector on the  $b \rightarrow s\gamma\gamma$  amplitude. We, therefore, allow ourselves to disregard potential contributions that can change our results for  $BR(B_s \rightarrow \gamma\gamma)$  and  $BR(B \rightarrow X_s\gamma\gamma)$  by less than an order of magnitude, such as the effects of RPC SUSY mentioned above, QCD corrections and possible long-distance non-perturbative effects. The latter includes strong resonance effects such as  $B \rightarrow X_s\eta(\eta') \rightarrow X_s\gamma\gamma$  and the even more significant  $b \rightarrow s\eta_c \rightarrow s\gamma\gamma$  - estimated in [6] to have a width about six times larger than the short distance width. These resonant contributions can, however, be essentially removed using appropriate kinematical cuts on the two photons invariant mass, with little impact on the short distance width [6].

As for the RPC SUSY contribution, one can alternatively assume that the RPC SUSY parameter space falls into a “corner” for which its effect on the  $b \rightarrow s\gamma\gamma$  amplitude is much smaller than the RPV effect reported in this work. Besides, whether such a corner of the RPC SUSY parameter space is realized or not in nature, our results do not justify a detailed analysis which includes the above elements. Nonetheless, in order to appreciate the relative size of the RPV SUSY effect, we will include the EW SM contribution, defining the total width as (for each of the two photon decays):

$$\Gamma = \Gamma_{SM} + \Gamma_{RPV} + \Gamma_{interference} , \quad (2)$$

where the pure SM and RPV contributions as well as their interference will be explicitly given.

As in [5, 6, 8], the width  $\Gamma(B \rightarrow X_s\gamma\gamma)$  will be approximated by the quark process  $\Gamma(b \rightarrow s\gamma\gamma)$  and the branching ratio will be defined via:

$$BR(B \rightarrow X_s\gamma\gamma) \equiv \frac{\Gamma(b \rightarrow s\gamma\gamma)}{\Gamma(b \rightarrow ce\nu_e)} \times BR^{exp}(B \rightarrow X_c e \nu_e) , \quad (3)$$

where  $\Gamma(b \rightarrow ce\nu_e) = 3 \times 10^{-5}$  eV is calculated at tree-level (also without QCD corrections) and we take  $BR^{exp}(B \rightarrow X_c e \nu_e) = 0.11$  [11].

Following [4],  $\Gamma(B_s \rightarrow \gamma\gamma)$  will be calculated using the static quark approximation. The corresponding branching ratio will be defined as:

$$BR(B_s \rightarrow \gamma\gamma) \equiv \frac{\Gamma(B_s \rightarrow \gamma\gamma)}{\Gamma_{tot}(B_s)} , \quad (4)$$

where  $\Gamma_{tot}(B_s)$  is the total  $B_s$  width given by its lifetime  $\tau(B_s) = 1.46 \times 10^{-12}$  sec [11].

Furthermore, we define the ratios

$$R_{s\gamma\gamma}^M \equiv \frac{BR^M(B \rightarrow X_s\gamma\gamma)}{BR^{SM}(B \rightarrow X_s\gamma\gamma)} , \quad R_{\gamma\gamma}^M \equiv \frac{BR^M(B_s \rightarrow \gamma\gamma)}{BR^{SM}(B_s \rightarrow \gamma\gamma)} , \quad R_\gamma^M \equiv \frac{BR^M(B \rightarrow X_s\gamma)}{BR^{SM}(B \rightarrow X_s\gamma)} , \quad (5)$$

where  $M$  denotes the model used for the calculation (RPV in our case). Thus, the more  $R_{s\gamma\gamma}^M$ ,  $R_{\gamma\gamma}^M$  or  $R_\gamma^M$  become larger than 1, the more pronounced will the effects of new physics be in the decays  $B \rightarrow X_s\gamma\gamma$ ,  $B_s \rightarrow \gamma\gamma$  or  $B \rightarrow X_s\gamma$ , respectively.

Naively, one would expect the one-loop diagrams for  $b \rightarrow s\gamma\gamma$  to be closely related to those for  $b \rightarrow s\gamma$  by “erasing” one photon line. In what follows we will refer to these type of diagrams (shown in Fig. 1) as  $\lambda$ -*reducible* diagrams. In this case, there will be a strong correlation between the two and the one photon  $b \rightarrow s$  decays. In other words, for a given new physics  $M$ , we expect the  $\lambda$ -*reducible* diagrams to yield  $R_{s\gamma\gamma}^M$ ,  $R_{\gamma\gamma}^M \sim R_\gamma^M$ , and so the rather stringent constraint from the experimentally well measured decay  $b \rightarrow s\gamma$  will project to the two photon decays  $B \rightarrow X_s\gamma\gamma$  and  $B_s \rightarrow \gamma\gamma$  as well. Indeed, such a strong correlation between the two and one photon  $b \rightarrow s$  decays was found in the RPC SUSY case [7] and for the 2HDM [8]. In contrast, as will be shown in this paper, in the RPV SUSY case there is a new class of diagrams (shown in Fig. 2) which are topologically different, thus contributing at one-loop only to  $b \rightarrow s\gamma\gamma$  and not to  $b \rightarrow s\gamma$ . These diagrams were introduced by us [12] for the related LFV two photon decay  $\mu \rightarrow e\gamma\gamma$  in [12]. Following [12], these diagrams will be named  $\lambda$ -*irreducible*, since one cannot turn them into  $b \rightarrow s\gamma$  diagrams by “erasing” one photon line. Therefore, at least in principle, in the RPV case the  $\lambda$ -*irreducible* diagrams can have a large effect in  $B \rightarrow X_s\gamma\gamma$  or in  $B_s \rightarrow \gamma\gamma$ , while giving a much smaller (i.e., two-loop) contribution to  $B \rightarrow X_s\gamma$ . Again, such an anti-correlation can be parametrized by the ratios  $R_{s\gamma\gamma}^{RPV}$ ,  $R_{\gamma\gamma}^{RPV}$  and  $R_\gamma^{RPV}$ , since in this case (i.e.,  $\lambda$ -*irreducible* RPV effect) it is possible to have  $R_{s\gamma\gamma}^{RPV}$ ,  $R_{\gamma\gamma}^{RPV} \gg R_\gamma^{RPV}$ .

Indeed, we find that the dominant RPV effect is generated by the  $\lambda$ -*irreducible* diagram with a  $\tau$ -loop, which has a negligible effect on  $b \rightarrow s\gamma$ , i.e., giving  $R_\gamma^{RPV} \ll 1$ . For the case of  $B \rightarrow X_s\gamma\gamma$ , this diagram gives  $R_{s\gamma\gamma}^{RPV} \sim 5$ , so there is no dramatic change to the rate. Nonetheless, in spite of the rather marginal RPV effect, we find that other

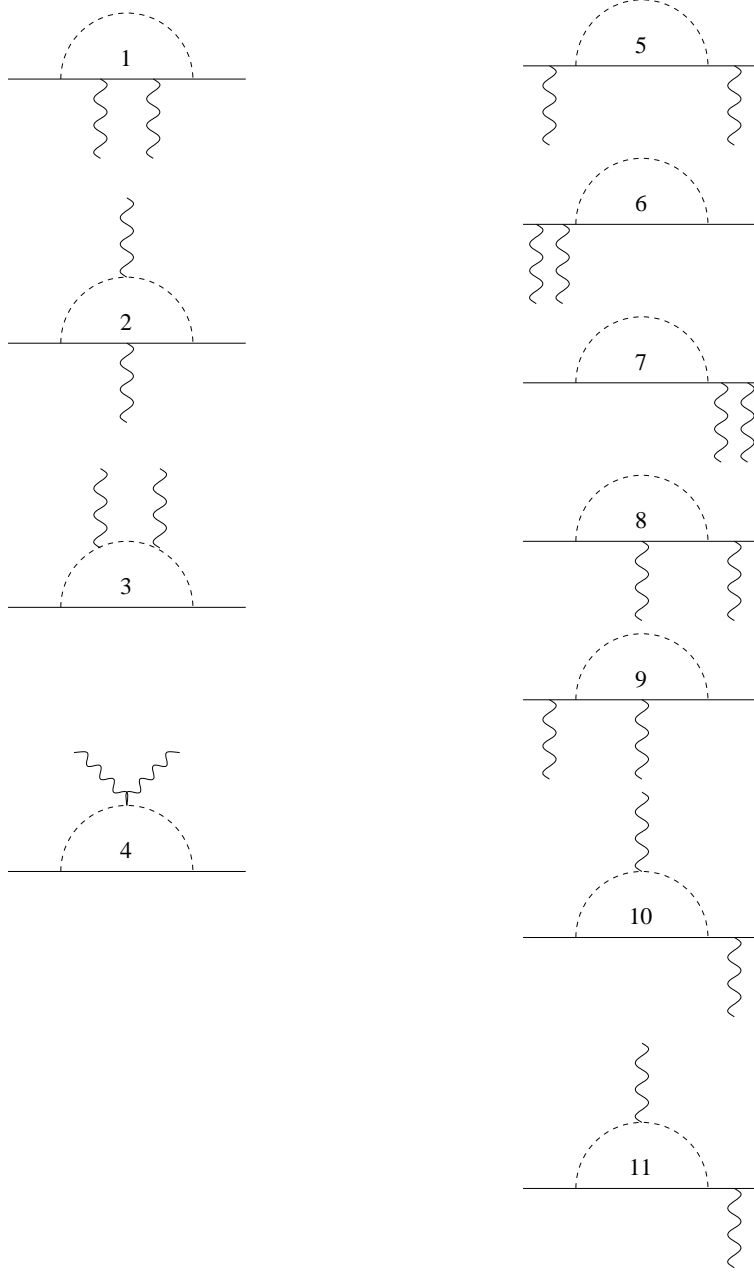


FIG. 1: The full set of  $\lambda$ -reducible one-loop diagrams for  $b \rightarrow s\gamma\gamma$ . Diagrams 1-4 are 1-particle-irreducible (1PI) and diagrams 5-11 are 1-particle-reducible (1PR) diagrams. The particles in the loops may be neutrino and  $d$ -type squark (then only diagrams 3-7, 10, and 11 contribute), sneutrino and  $d$ -type quark (then only diagrams 1 and 5-9 contribute), lepton and  $u$ -type squark, and slepton and  $u$ -type quark. All the scalar-fermion-fermion vertices are RPV. In all the diagrams except 4, the interchange of photons is implied.

observables such as the shape of the energy distribution of the two photons and the value of a Forward-Backward-Asymmetry (FBA) (with respect to the softer photon), are significantly distinguishable from their SM counterparts in the presence of the  $\lambda$ -irreducible RPV effect and can, therefore, be used to disentangle the new physics contribution to  $B \rightarrow X_s\gamma\gamma$ . Let us also mention that we adhere to the single coupling scheme i.e., we consider only one pair of couplings at a time.

As for the decay  $B_s \rightarrow \gamma\gamma$ , we find that the  $\lambda$ -irreducible diagram with a  $\tau$ -loop can enhance its branching ratio by more than an order of magnitude. In particular,  $R_{\gamma\gamma}^{RPV} \sim 16.6$ , where the enhancement comes from the pure RPV contribution since the interference of the  $\lambda$ -irreducible  $\tau$ -loop diagram with the SM diagrams is much smaller.

The paper is organized as follows: In section II we calculate the branching ratio, the energy distribution of the two photons and the FBA for  $B \rightarrow X_s\gamma\gamma$ . In section III we calculate the branching ratio for the decay  $B_s \rightarrow \gamma\gamma$  and in section IV we summarize our results.

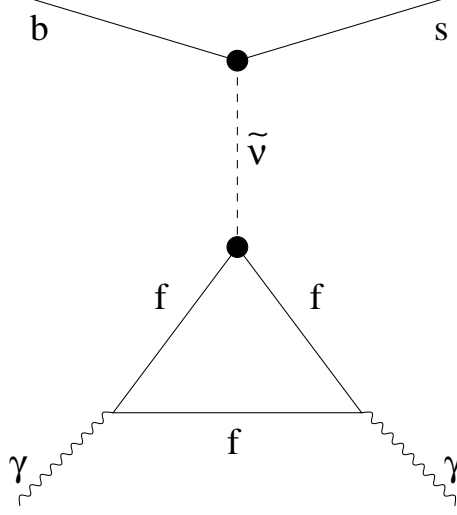


FIG. 2: A typical  $\lambda$ -irreducible diagram for  $b \rightarrow s\gamma\gamma$ . The full circles denote RPV vertices. Interchange of photons is implied, and  $f$ ,  $\tilde{\nu}$  stand for a fermion with weak isospin  $-1/2$ , sneutrino, respectively.

## II. $B \rightarrow X_s \gamma\gamma$

### A. Calculational setup

For the calculation of the  $b(p_b) \rightarrow s(p_s)\gamma(k_1)\gamma(k_2)$  decay rate we will employ the same cuts as in [5]. In particular, the integration domain  $D$  is defined using the following cuts:

1. The invariant mass of any pair of particles is constrained via:

$$(p_s + k_1)^2 > cm_b^2, \quad (p_s + k_2)^2 > cm_b^2, \quad (k_1 + k_2)^2 > cm_b^2, \quad (6)$$

where all momenta are taken in the  $b$ -quark rest frame. The "cutoff" parameter  $c$  will be set to 0.01 or 0.02.

2. The angle between any pair of the outgoing particles is restricted to be larger than  $20^\circ$ .
3. The energy of each of the photons is cut off from below at 100 MeV, to avoid IR divergences from too soft photons in the final state.

Thus,  $\Gamma(b \rightarrow s\gamma\gamma)$  is calculated from

$$\Gamma(b \rightarrow s\gamma\gamma) = \frac{1}{2} \int_D \frac{dE' d\omega}{64\pi^3 m_b} |\mathcal{M}|^2, \quad (7)$$

where the factor of half is included to take into account the identical photons in the final state and  $\int_D$  denotes an integration over the domain  $D$  defined above. Also,  $E'$  and  $\omega$  are  $s$ -quark and  $\gamma$  energies, respectively. The RPV amplitudes for each diagram are defined as:

$$\mathcal{M}_i = \frac{\alpha G_\lambda}{\sqrt{2}\pi} \bar{s} \mathcal{O}_i b, \quad (8)$$

where  $G_\lambda/\sqrt{2} \equiv (\lambda'\lambda')_i/(8M_i^2)$ ,  $(\lambda'\lambda')_i$  denotes the product of the trilinear RPV coupling relevant for the amplitude  $\mathcal{M}_i$  and  $M_i$  is the mass of the corresponding sparticle. Thus, in (7)  $\mathcal{M} = \sum_i \mathcal{M}_i$  is to be understood.

The quark masses are taken to be:  $m_t = 175$  GeV,  $m_b = 4.5$  GeV,  $m_c = 1.5$  GeV, and (as in [5])  $m_s$  is taken to be 0.15 GeV in  $\mathcal{M}$  and 0.45 GeV in the integration limits.

The branching ratio for the decay  $B \rightarrow X_s \gamma\gamma$ , subject to the above integration domain for  $b \rightarrow s\gamma\gamma$ , is then calculated using (3).

In addition to the rate, we will consider the energy distribution of the two outgoing photons  $1/\Gamma d\Gamma/d\hat{s}$ , where

$$\hat{s} \equiv \frac{(k_1 + k_2)^2}{m_b^2} = \frac{m_b^2 + m_s^2 - 2m_b E'}{m_b^2}, \quad (9)$$

and the FBA defined as follows [5]:<sup>[1]</sup>

$$A_{FB} = \frac{\Gamma(\cos\theta \geq 0) - \Gamma(\cos\theta < 0)}{\Gamma(\cos\theta \geq 0) + \Gamma(\cos\theta < 0)}, \quad (10)$$

where  $\theta$  is the angle between the  $s$ -quark and the softer photon.

### B. $B \rightarrow X_s \gamma \gamma$ in the SM

The SM width for  $B \rightarrow X_s \gamma \gamma$  is calculated using (3), with the SM amplitude given in [4] and with the set of cuts and input parameters outlined in the previous section. Our SM results for the branching ratio and for the FBA are given in Table I, where the contributions from the pure 1-particle reducible (1PR) and 1-particle irreducible (1PI) diagrams, as well as their interference are explicitly listed. The energy distribution of the two-photons in the SM will be given and compared to the RPV one in the next sections.

	$BR(B \rightarrow X_s \gamma \gamma) \times 10^7$				$A_{FB}$
	Total	1PR	1PI	Interference	
$c = 0.01$	1.34	1.02	0.24	0.08	0.66
$c = 0.02$	1.18	0.86	0.24	0.08	0.63

TABLE I: The SM branching ratio and the FBA [defined in (10)], for the decay  $B \rightarrow X_s \gamma \gamma$ . The cutoff  $c$  is defined in (6).

We note that our results for the SM total branching ratio are about 15% smaller than the results obtained in [5] (recall that we are using the same set of cuts and inputs). This disagreement results only from the pure 1PR contribution, since our pure 1PI and 1PI-1PR interference parts are in perfect agreement with [5]. Also, our results for the FBA in the SM agree with [5] up-to a few percent.

### C. RPV couplings

Extensive reviews on the constraints for RPV parameters can be found in [13, 14, 15, 16]. We note, however, that some of the entries in [13, 14, 15, 16] require a renewal which we carry out for combinations of  $\lambda$ 's relevant for the  $b \rightarrow s \gamma \gamma$  transition of our interest. In particular, in what follows we will use limits obtained from  $b \rightarrow s \ell^+ \ell^-$  [17], from  $B \rightarrow PP$  [18], where  $P$  is a pseudoscalar meson (this includes  $B \rightarrow \pi\pi$ ,  $B \rightarrow K\pi$ , and  $B \rightarrow K\bar{K}$  decays), from  $B \rightarrow \phi K_s$  [19] and from  $B \rightarrow \phi\phi$  and  $B \rightarrow \phi\pi$  [20]. Most of these decays are generated at one-loop in the SM but at tree level in RPV SUSY. Some of the exclusive processes mentioned above require modeling. For example, in [18] the so-called factorization approximation was used. Therefore, some of these bounds are uncertain to the level of the approximation made. In the following, we will discuss in more detail the limits on the individual RPV coupling products which apply to the specific diagram or set of diagrams being considered.

### D. Contribution from $\lambda$ -irreducible diagrams

As mentioned earlier, the  $\lambda$ -irreducible diagrams with the topology shown in Fig. 2 could, in principle, give a substantial contribution to  $b \rightarrow s \gamma \gamma$ , almost without any effect on  $b \rightarrow s \gamma$ , since they cannot be turned into  $b \rightarrow s \gamma$  diagrams by removing one photon line. These type of diagrams were also employed in [12] for the LFV decay  $\mu \rightarrow e \gamma \gamma$ . Thus, for the  $\lambda$ -irreducible topology,  $\Gamma(b \rightarrow s \gamma \gamma)$  can be obtained from  $\Gamma(\mu \rightarrow e \gamma \gamma)$  simply by interchanging  $m_\mu \rightarrow m_b$  and  $m_e \rightarrow m_s$  and taking the appropriate RPV couplings. We, therefore, use here the results of [12], with the set of kinematical cuts that defines our integration domain.

Let us first consider the case of  $f = d$  in the loop of Fig. 2. This diagram is proportional to the RPV couplings  $\lambda'_{23}\lambda'_{i11}$  or  $\lambda'_{32}\lambda'_{i11}$  (depending on the chirality of the  $b$  and  $s$ -quarks), which are constrained by the tree-level  $b \rightarrow s d \bar{d}$  [18] (note that  $b \rightarrow s d \bar{d}$  can be obtained from the  $\lambda$ -irreducible diagram by "chopping" the loop and turning it into a tree-level diagram). The constraint from [18] induces some uncertainty from the modeling of the exclusive decay  $B \rightarrow K\pi$  (when calculated from the quark-level process  $b \rightarrow s d \bar{d}$ ). Disregarding such uncertainties, we obtain  $BR(b \rightarrow s \gamma \gamma) \sim 10^{-9}$ , *i.e.* about two orders of magnitudes smaller than the SM prediction.

[1] The FBA is usually defined for processes with distinct final particles, such as  $\ell^+$  and  $\ell^-$  in the decay  $b \rightarrow s \ell^+ \ell^-$ . Since in our case there are two identical particles in the final state, the usual definition of a FBA does not apply.

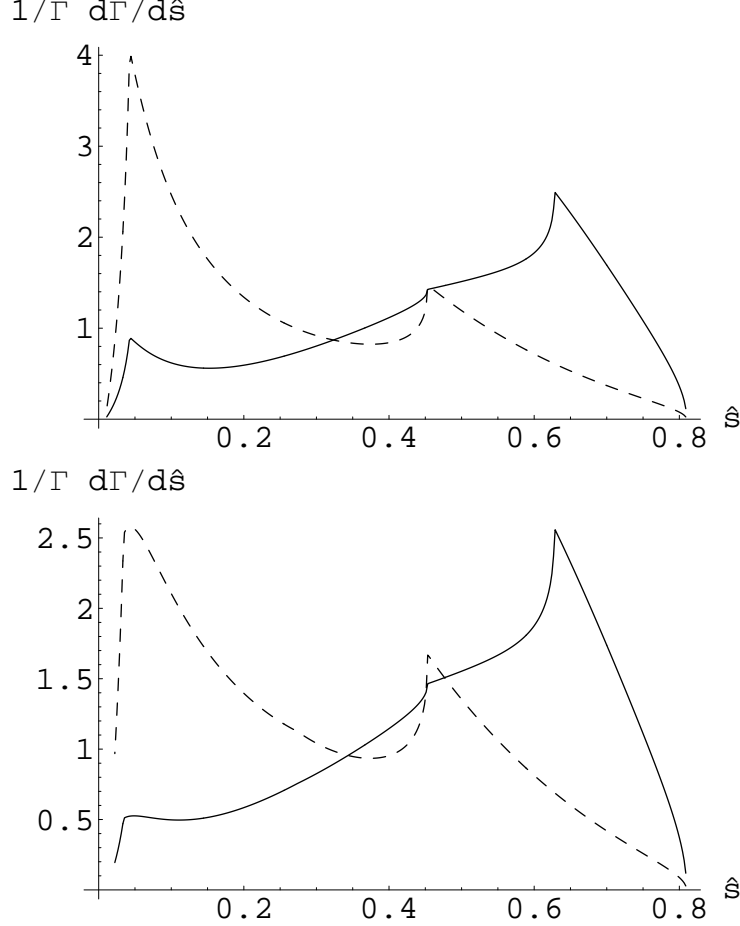


FIG. 3: The two photons energy distribution  $1/\Gamma \, d\Gamma/d\hat{s}$ , as a function of  $\hat{s} \equiv (k_1 + k_2)^2/m_b^2$ , in the SM (dashed-line) and in the SM+RPV case (solid-line) for the  $\lambda$ -irreducible diagram with the  $\tau$ -loop, with  $\lambda'_{232}\lambda_{233} = 0.0234$ . For the upper graph  $c = 0.01$  while  $c = 0.02$  for the lower one. The low  $\hat{s}$  peak is due to bremsstrahlung and the cuts in Eqn. (6). The other two sharp peaks correspond to threshold openings at  $\hat{s} = 4m_\tau^2/m_b^2$  and  $\hat{s} = 4m_c^2/m_b^2$ .

The effect of the  $\lambda$ -irreducible diagrams with  $f = s$  or  $b$  in the loop is much smaller than that with  $f = d$ , when the existing constraints on the relevant  $\lambda'\lambda'$  product are imposed. Besides, the couplings  $\lambda'\lambda'$  relevant for  $f = s$  or  $b$  also contribute to the  $\lambda$ -reducible diagrams, which give a larger effect for these specific couplings (see next section).

For the case of  $f = e, \mu$ , there are rather stringent constraints coming from the inclusive  $b \rightarrow sl^+l^-$  [17]. Thus, for example, the BR for  $b \rightarrow s\gamma\gamma$  calculated with the muon loop is  $\sim \mathcal{O}(10^{-13})$  and even smaller for the electron loop.

For the  $\lambda$ -irreducible diagram with the  $\tau$  loop, the situation is different. The relevant  $\lambda'\lambda$  products that can drive the  $\tau$ -loop  $\lambda$ -irreducible diagram are:  $\lambda'_{232}\lambda_{233}$  or  $\lambda'_{223}\lambda_{233}$  and  $\lambda'_{123}\lambda_{133}$  or  $\lambda'_{132}\lambda_{133}$ , for the  $\tilde{\nu}_\mu$  and  $\tilde{\nu}_e$  exchanges, respectively. However, since  $\lambda_{133}$  is severely constrained by the bound on the electron neutrino mass [21],  $\lambda_{133} < 0.006$ , the contribution from the  $\tilde{\nu}_e$  exchange is negligible. Moreover, since the current bounds imply that  $\lambda'_{223}\lambda_{233} < \lambda'_{232}\lambda_{233}$  (see [13, 14]), we will investigate only the effect of the  $\lambda'_{232}\lambda_{233}$  coupling, for which the current limit is  $\lambda'_{232}\lambda_{233} < 0.0234$  for a 100 GeV sparticle mass [13] (note that the constraint on  $\lambda'_{232}\lambda_{233}$  reported in [14] is weaker). This constraint results from a combination of bounds coming from  $Z$ -decays [22] and  $\tau$ -decays [23]. We note that there is no useful experimental limit on  $b \rightarrow s\tau^+\tau^-$  which could in principle impose a stronger bound on this coupling product. Thus, taking  $\lambda'_{232}\lambda_{233} = 0.0234$ , we list in Table II our numerical results for the maximal  $\tau$ -loop  $\lambda$ -irreducible contribution to the  $BR(B \rightarrow X_s\gamma\gamma)$ , to the FBA  $A_{FB}$  defined in (10) and to the ratio  $R_{s\gamma\gamma}^{RPV}$  defined in (5). We see that in the  $\tau$ -loop case, the branching ratio for  $B \rightarrow X_s\gamma\gamma$  can reach  $\sim 6 \times 10^{-7}$ , which is about 5 times larger than the SM value. This enhancement arises from the pure RPV contribution since the interference between the RPV and the SM contributions is negligible in this case (i.e., less than 1% of the total rate).

We also find that, for the  $\lambda$ -irreducible diagram with the  $\tau$ -loop, the FBA ( $A_{FB} \sim 0.45$ , see Table II) as well as the photons energy distribution  $1/\Gamma \, d\Gamma/d\hat{s}$  (shown in Fig. 3) are significantly different from their values in the SM. Therefore, these quantities may prove useful for disentangling the  $\lambda$ -irreducible RPV effect in  $B \rightarrow X_s\gamma\gamma$ . Let us also mention that we adhere to the one-coupling scheme, i.e., assuming one contribution of a pair of RPV couplings at a time.

	RPV coupling	$(\lambda'\lambda)_{max}$ [13]	$BR(B \rightarrow X_s \gamma \gamma) \times 10^7$				$A_{FB}$	$R_{s\gamma\gamma}^{RPV}$
			SM	RPV	Interference	Total		
$c = 0.01$	$\lambda'_{232}\lambda_{233}$	0.0234	1.34	4.81	$\times$	6.15	0.46	4.6
$c = 0.02$	"-"	"-"	1.18	4.81	$\times$	5.99	0.45	5.1

TABLE II:  $BR(B \rightarrow X_s \gamma \gamma) \times 10^7$  for the  $\lambda$ -irreducible diagram with the  $\tau$ -loop case.  $R_{s\gamma\gamma}^{RPV}$  is defined in (5) and  $A_{FB}$  is defined in (10). The sneutrino mass is assumed to be 100 GeV.  $\times$  means that the contribution is of  $\mathcal{O}(1\%)$  (or smaller) of the total rate. The cutoff  $c$  is defined in (6).

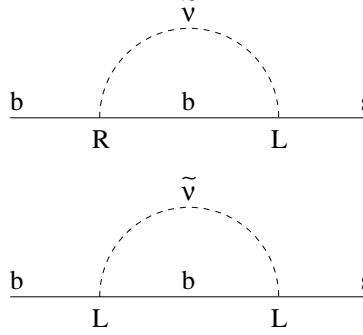


FIG. 4: The chirality non-flip (upper part) and chirality flip (lower part) diagrams. L and R denote left and right chirality projectors, respectively. The external photons may be attached to any charged line.

### E. Contribution from $\lambda$ -reducible diagrams

The full set of one-loop  $\lambda$ -reducible RPV diagrams for  $b \rightarrow s\gamma\gamma$  is given in Fig. 1. These diagrams can be classified according to the RPV coupling involved. For example, for  $\lambda'_{ij2}\lambda'_{ij3}$  all the  $\lambda$ -reducible diagrams are relevant, while for  $\lambda'_{i2k}\lambda'_{i3k}$  only the diagrams with  $d$ -quark-sneutrino ( $d - \tilde{\nu}$ ) or  $d$ -squark-neutrino ( $\tilde{d} - \nu$ ) in the loop contribute. In addition, the  $\lambda$ -reducible diagrams can be further subdivided (shown in Fig. 4), into "flip"-diagrams and "non-flip" diagrams according to whether the incoming  $b$ -quark and outgoing  $s$ -quark have different or the same chiralities, respectively. The flip diagrams are important only for  $j = 3$  or  $k = 3$ , where the mass insertion for the chirality flip is  $m_b$  (i.e., the internal quark in the loop is the  $b$ -quark). The classification of the  $\lambda$ -reducible diagrams is given in Table III.

loop particles RPV couplings	1PI				1PR			
	$d - \tilde{\nu}$ ( $\lambda'_{ij3}\lambda'_{ij2},$ $\lambda'_{i3k}\lambda'_{i2k}$ )	$\nu - \tilde{d}$ ( $\lambda'_{ij3}\lambda'_{ij2},$ $\lambda'_{i3k}\lambda'_{i2k}$ )	$u - \tilde{\ell}$ ( $\lambda'_{ij3}\lambda'_{ij2}$ )	$\ell - \tilde{u}$ ( $\lambda'_{ij3}\lambda'_{ij2}$ )	$d - \tilde{\nu}$ ( $\lambda'_{ij3}\lambda'_{ij2},$ $\lambda'_{i3k}\lambda'_{i2k}$ )	$\nu - \tilde{d}$ ( $\lambda'_{ij3}\lambda'_{ij2},$ $\lambda'_{i3k}\lambda'_{i2k}$ )	$u - \tilde{\ell}$ ( $\lambda'_{ij3}\lambda'_{ij2}$ )	$\ell - \tilde{u}$ ( $\lambda'_{ij3}\lambda'_{ij2}$ )
non-flip	1	3,4	1-4	1-4	5-9	5-7,10,11	5-11	5-11
flip	$\checkmark$	$\times$	$\times$	$\times$	$\checkmark$	$\times$	$\times$	$\times$

TABLE III: Classification of  $\lambda$ -reducible diagrams. The numbers in the "non-flip" row denote those diagrams in Fig. 1 which belong to the non-flip category. In the "flip" row  $\checkmark$  is inserted if the relevant diagram can have a chirality flip, and  $\times$  if not. Also, 1PI and 1PR stand for one-particle-irreducible and one-particle-reducible diagrams, respectively.

We find that the maximal effect (i.e., using the maximal allowed values for the corresponding RPV couplings) of any given non-flip diagram is always about two order of magnitude smaller than the contribution generated by the dominant flip diagrams with the  $b - \tilde{\nu}$  loops. Nonetheless, for completeness, we give below the derivation of the amplitudes for the largest non-flip contributions.

#### 1. Non-flip diagrams

For the non-flip diagrams we define:

$$Q_3 + \Delta Q_3 = i\epsilon^{\mu\nu\xi\alpha}\gamma_\alpha L(k_1 - k_2)_\xi + i\frac{k_{1\xi}k_{2\eta}}{k_1 \cdot k_2}(\epsilon^{\mu\xi\eta\alpha}k_1^\nu - \epsilon^{\nu\xi\eta\alpha}k_2^\mu)\gamma_\alpha L, \quad (11)$$

and

$$W = -\left[\left(\frac{p_s^\nu}{p_s \cdot k_2} - \frac{p_b^\nu}{p_b \cdot k_2}\right)\sigma(\mu, k_1) + \left(\frac{p_s^\mu}{p_s \cdot k_1} - \frac{p_b^\mu}{p_b \cdot k_1}\right)\sigma(\nu, k_2)\right]$$

$$+\frac{i}{2}\left[\left(\frac{1}{p_s \cdot k_2} - \frac{1}{p_b \cdot k_1}\right)\sigma(\nu, k_2)\sigma(\mu, k_1) + \left(\frac{1}{p_s \cdot k_1} - \frac{1}{p_b \cdot k_2}\right)\sigma(\mu, k_1)\sigma(\nu, k_2)\right], \quad (12)$$

where  $\sigma(\mu, k) \equiv \sigma^{\mu\rho}k_\rho$  and  $\sigma^{\mu\nu} = \frac{1}{2i}[\gamma^\mu, \gamma^\nu]$ . Then, using the prescription given in section II A, the operators  $\mathcal{O}$  [defined in (8)], for the non-flip diagrams that give the largest non-flip effect are given in Table IV, wherein the non-flip contributions are further classified according to the particles/sparticles exchanged in the loops.

Loop particles	$\mathcal{O}$
$\bar{b} - \nu$	$-\frac{i}{54}W(m_b L + m_s R)$
$b - \bar{\nu}$ (non-flip)	$-\frac{2}{9}(Q_3 + \Delta Q_3)\delta_3 + \frac{i}{27}W(m_b L + m_s R)$
$\tilde{c} - \ell$	$-2(Q_3 + \Delta Q_3)\delta_3 + \frac{4i}{27}W(m_b L + m_s R)$
$c - \tilde{\ell}$	$-\frac{8}{9}(Q_3 + \Delta Q_3)\delta_3 - \frac{7i}{54}W(m_b L + m_s R)$
$t - \tilde{\ell}$	$-\frac{1}{3}F'_2(z^2)W(m_b L + m_s R)$ , where $F'_2(x) = \frac{7-12x-3x^2+8x^3-6x(-2+3x)\log x}{18(x-1)^4}$ and $z = m_t/M$

TABLE IV: The operators appearing in the  $\lambda$ -*reducible* amplitudes following the definition in (8).  $Q_3 + \Delta Q_3$  and  $W$  are given in (11) and (12).  $M$  is the sparticle mass.

As mentioned above, the contribution from the non-flip operators in Table IV is always subdominant compared to that coming from the  $b - \bar{\nu}$  flip diagrams. In particular, for the non-flip case we find that the typical branching ratio is  $BR(B \rightarrow X_s \gamma \gamma) \sim 10^{-9}$ . Let us, therefore, proceed with the  $b - \bar{\nu}$  flip diagrams.

## 2. Flip diagrams

The dominant flip diagrams are obtained from the  $b - \bar{\nu}$  loops and are, therefore, proportional to either  $\lambda'_{323}\lambda'_{333}$  or  $\lambda'_{332}\lambda'_{333}$ , depending on the chiralities of the incoming  $b$ -quark and outgoing  $s$ -quark.<sup>[2]</sup> The constraints on these RPV coupling products come from  $b \rightarrow c l \nu$  and  $B_s - \bar{B}_s$  mixing, see [19]. The expression for the amplitude of these flip diagrams is, unfortunately, too long to be useful for the reader and will not be given here.<sup>[3]</sup>

The calculation for the flip diagrams was performed using the Mathematica package. The numerical results are presented in Table V, where all interferences were taken to be constructive, by adjusting the sign of the RPV couplings.

	RPV coupling	$(\lambda'\lambda')_{max}$ [19]	$BR(B \rightarrow X_s \gamma \gamma) \times 10^7$	$A_{FB}$	$R_{s\gamma\gamma}^{RPV}$
$c = 0.01$	$\lambda'_{323}\lambda'_{333}$	0.0033	1.34 1.02 2.11 4.47	0.73	3.3
	$\lambda'_{332}\lambda'_{333}$	0.0025	-" 0.58 0.05 1.97	0.7	1.5
$c = 0.02$	$\lambda'_{323}\lambda'_{333}$	0.0033	1.18 0.86 1.8 3.84	0.7	3.3
	$\lambda'_{332}\lambda'_{333}$	0.0025	-" 0.49 0.04 1.71	0.66	1.5

TABLE V: Maximal  $BR(B \rightarrow X_s \gamma \gamma) \times 10^7$ ,  $A_{FB}$  and  $R_{s\gamma\gamma}^{RPV}$ , for the  $\lambda$ -*reducible* flip diagrams with the  $b - \bar{\nu}$  loops. The cutoff  $c$  is defined in (6).

From Table V we see that the largest effect, which comes from the interference of the RPV  $b - \bar{\nu}$  flip diagrams ( $\propto \lambda'_{323}\lambda'_{333}$ ) with the SM ones, is not quantitatively much different from the pure SM prediction and is smaller than the  $\lambda$ -*irreducible* effect with the  $\tau$ -loop. The same conclusion holds for the overall SM+RPV FBA which remains close to its SM value.

In Figs. 5 and 6 we show the energy distribution of the two photons,  $1/\Gamma d\Gamma/d\hat{s}$ , in the pure SM and for the SM + RPV flip diagrams with  $\lambda'_{332}\lambda'_{333} = 0.0025$  and  $\lambda'_{323}\lambda'_{333} = 0.0033$ , respectively. As can be seen from these figures, the shape of the SM energy distribution remains almost unchanged when the RPV flip diagrams are included.

Therefore, to conclude this section, the largest RPV  $\lambda$ -*reducible* contribution to  $BR(B \rightarrow X_s \gamma \gamma)$ , which comes from flip diagrams with  $b - \bar{\nu}$  loops, is somewhat smaller than the RPV  $\lambda$ -*irreducible* contribution. Moreover, within the  $\lambda$ -*reducible* topology, the FBA and the photons energy distribution are essentially indistinguishable from the SM, whereas the  $\lambda$ -*irreducible* topology can significantly alter the value and shape of these quantities.

## III. $B_s \rightarrow \gamma\gamma$

For the calculation of  $\Gamma(B_s \rightarrow \gamma\gamma)$  we adopt the static quark approximation [4], where  $m_{B_s} = m_b + m_s$  and both  $b$  and  $s$  have zero 3-momenta in the rest frame of the decaying  $B_s$  meson, in which case the photons are emitted

[2] Note that the  $\lambda$ -*reducible* diagrams with RPV couplings corresponding to  $b$  and  $s$ -quark in the loops, contribute also to the  $\lambda$ -*irreducible* topology. However, for these specific couplings, the  $\lambda$ -*reducible* effect exceeds the  $\lambda$ -*irreducible* one.

[3] The expression for the  $b - \bar{\nu}$  flip diagrams can be ordered by e-mail from S.G.



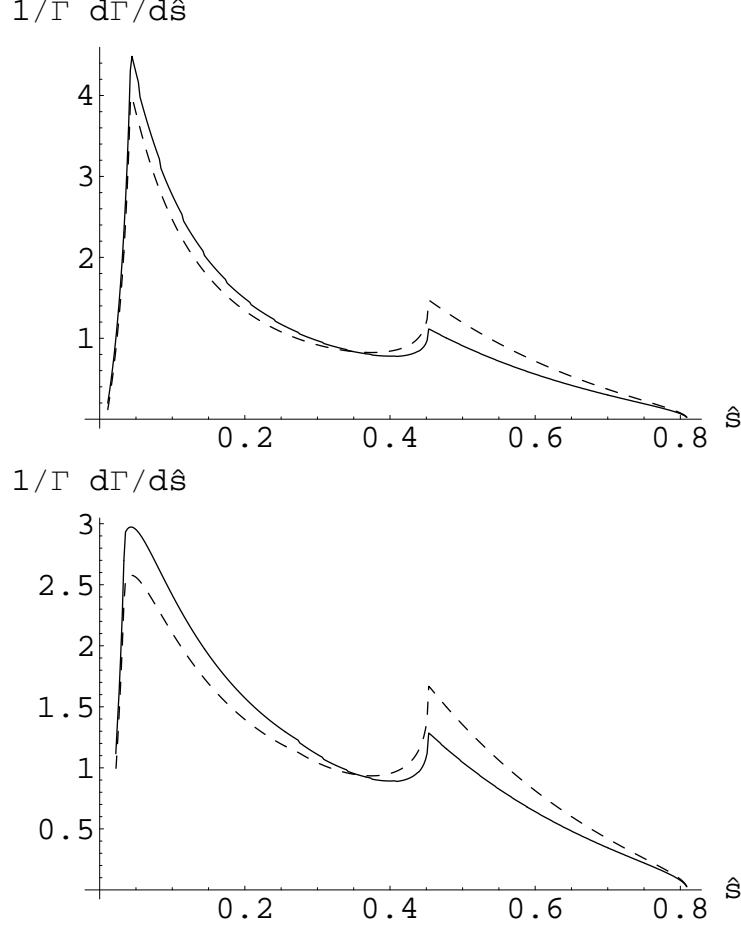


FIG. 5:  $1/\Gamma \, d\Gamma/d\hat{s}$  as a function of  $\hat{s}$  for SM (dashed) and SM+RPV (solid) for  $\lambda$ -reducible diagrams with  $\lambda'_{i32}\lambda'_{i33} = 0.0025$ . Here  $c = 0.01$  for the upper graph and  $c = 0.02$  for the lower one. The cutoff  $c$  is defined in (6).

back-to-back with energies  $M_{B_s}/2$ . Since this model is non-relativistic, as in [4], we use the constituent mass for  $s$ -quark  $m_s = 500$  MeV.

The current matrix element is [4]:

$$\langle 0 | \bar{u}_s \gamma_\mu \gamma_5 u_b | B_s \rangle = -i f_{B_s} P_\mu, \quad (13)$$

where  $P = p_b - p_s$  is the  $B_s$ -meson 4-momentum and  $f_{B_s}$  is the  $B_s$ -meson decay constant.

From (13) one obtains

$$\langle 0 | \bar{u}_s \gamma_5 u_b | B_s \rangle = i f_{B_s} m_{B_s}. \quad (14)$$

In addition, the fact that

$$\langle 0 | \bar{u}_s \gamma_\mu u_b | B_s \rangle = 0, \quad (15)$$

can be used to simplify the calculation for the  $\lambda$ -reducible flip diagrams. For example, the term  $\bar{u}_s L \gamma_\mu \gamma_\nu u_b$  can be transformed to a combination of four terms:

$$\bar{u}_s L \gamma_\mu \gamma_\nu u_b = \frac{1}{m_b} \bar{u}_s L \gamma_\mu \gamma_\nu \not{p}_b u_b = \quad (16)$$

$$\frac{1}{m_b} (g_{\mu\nu} \bar{u}_s L \not{p}_b u_b + p_{b\nu} \bar{u}_s L \gamma_\mu u_b - p_{b\mu} \bar{u}_s L \gamma_\nu u_b + i \epsilon_{\mu\nu\rho\sigma} p_b^\rho \bar{u}_s L \gamma^\sigma u_b), \quad (17)$$

which, when put between vacuum and meson states as in (13), turns into

$$\bar{u}_s L \gamma_\mu \gamma_\nu u_b = \frac{i f_{B_s}}{2 m_b} (g_{\mu\nu} P \cdot p_b + p_{b\nu} P_\mu - p_{b\mu} P_\nu + i \epsilon_{\mu\nu\rho\sigma} p_b^\rho P^\sigma). \quad (18)$$

Thus, in the static quark approximation (18) amounts to

$$\bar{u}_s L \gamma_\mu \gamma_\nu u_b = \frac{i f_{B_s} m_{B_s}}{2} g_{\mu\nu}. \quad (19)$$

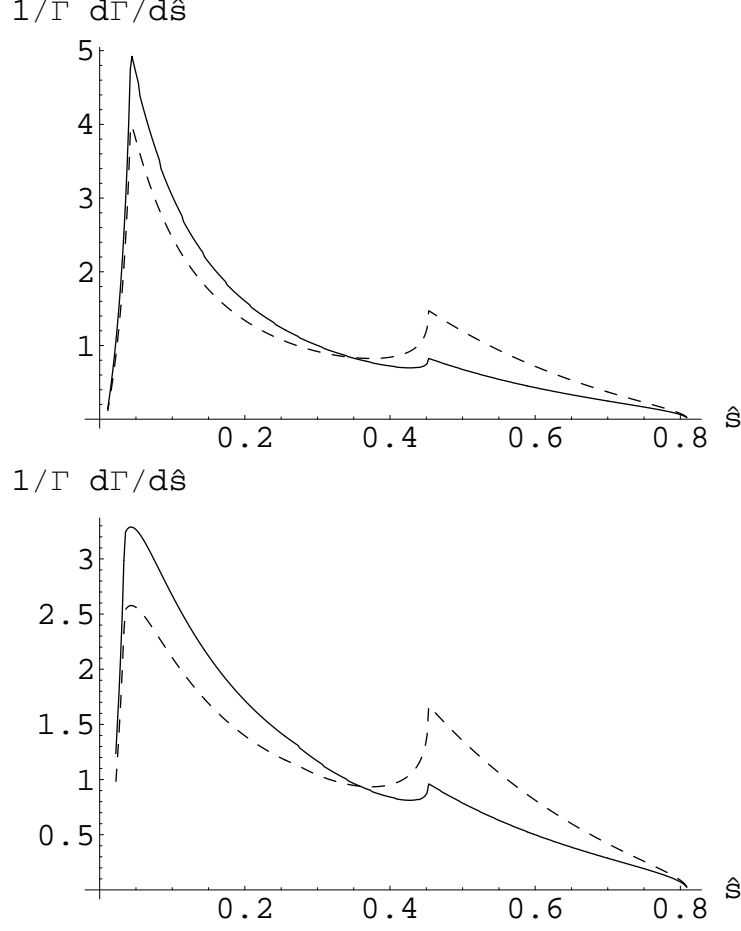


FIG. 6:  $1/\Gamma \, d\Gamma/d\hat{s}$  as a function of  $\hat{s}$  for SM (dashed) and SM+RPV (solid) for  $\lambda$ -reducible diagrams with  $\lambda'_{323}\lambda'_{333} = 0.0033$ . Here  $c = 0.01$  for the upper graph and  $c = 0.02$  for the lower one. The cutoff  $c$  is defined in (6).

Following the above procedure, the  $B_s \rightarrow \gamma\gamma$  amplitude can be parametrized as [4]:

$$\mathcal{M}_M = 2f_{B_s} \left[ B_M^+(k'_\mu k'_\nu - \frac{1}{2}m_{B_s}^2 g_{\mu\nu}) + B_M^- i\epsilon_{\mu\nu\rho\sigma} k^\rho k'^\sigma \right] \epsilon^\mu \epsilon'^\nu, \quad (20)$$

where the subscript  $M$  denotes the model used for the calculation. The decay width for  $B_s \rightarrow \gamma\gamma$  is then given by:

$$\Gamma^M(B_s \rightarrow \gamma\gamma) = f_{B_s}^2 \frac{m_{B_s}^3}{16\pi} (|B_M^+|^2 + |B_M^-|^2). \quad (21)$$

In the SM

$$B_{SM}^\pm = \frac{\alpha G_F}{\sqrt{2}\pi} A^\pm, \quad (22)$$

where the form factors  $A^+$  and  $A^-$  are defined in [4].

As in the case of  $B \rightarrow X_s \gamma\gamma$ , we find that the potentially largest RPV contribution to the width of  $B_s \rightarrow \gamma\gamma$  comes from the  $\lambda$ -irreducible diagram with the  $\tau$ -loop. In particular, this diagram gives an enhancement to  $\Gamma(B_s \rightarrow \gamma\gamma)$  which is about 100 or 10 times larger than the one obtained from the  $\lambda$ -reducible non-flip or flip diagrams, respectively.

The RPV form factors in the  $\lambda$ -irreducible case are:

$$B_{RPV}^{+;-} = \frac{\alpha m_{B_s}}{16\pi} \frac{i\lambda'_{232}\lambda_{233}}{m_\tau M_\nu^2} \cdot f_{1/2}(x); g_{1/2}(x), \quad (23)$$

with

$$\begin{aligned}
f_{1/2}(x) &= 2x \left[ 1 + (1-x) \arcsin^2 \left( \frac{1}{\sqrt{x}} \right) \right], \\
g_{1/2}(x) &= 2x \arcsin^2 \left( \frac{1}{\sqrt{x}} \right),
\end{aligned} \tag{24}$$

where  $M_{\tilde{\nu}}$  is the sneutrino mass and for the  $\tau$ -loop case  $x = (2m_\tau/m_{B_s})^2$ .

Our numerical results for the SM and the  $\lambda$ -*irreducible* RPV contributions to  $BR(B_s \rightarrow \gamma\gamma)$  [using (4)] are summarized in Table VI. The results were obtained with  $m_b = 4.8$  GeV,  $m_s = 0.5$  GeV,  $m_{B_s} = m_b + m_s$ ,  $V_{cb} = 0.04$  and  $f_{B_s} = 200$  MeV. The RPV couplings were taken at their maximal allowed values and the sneutrino mass was set to 100 GeV.

RPV from $\lambda$ - <i>irreducible</i> diagrams with the $\tau$ -loop					
RPV coupling	$(\lambda'\lambda')_{max}$ [13]	$BR(B_s \rightarrow \gamma\gamma) \times 10^7$			
		SM	RPV	Interference	Total
$\lambda_{232}\lambda_{233}$	0.0234	2.74	38.4	4.41	45.55
					16.62

TABLE VI:  $BR(B_s \rightarrow \gamma\gamma) \times 10^7$  in the SM and for the  $\lambda$ -*irreducible* diagrams with the  $\tau$ -loop. The sneutrino mass was set to 100 GeV. See also text.

We see that the enhancement from the  $\lambda$ -*irreducible*  $\tau$ -loop diagram is here particularly large:  $BR(B_s \rightarrow \gamma\gamma) \sim 5 \times 10^{-6}$ , about 16 times larger than the SM prediction (although still far below the experimental limit,  $1.48 \times 10^{-4}$  [11]). We also note that our numerical result for the SM branching ratio agrees with [4] after substituting our  $f_{B_s}$ ,  $V_{cb}$  and  $\tau(B_s)$  for the values used in [4].

#### IV. CONCLUSIONS

We have investigated the effects of RPV on the  $b \rightarrow s\gamma\gamma$  transition amplitude, focusing on the two-photon B decays  $B_s \rightarrow X_s\gamma\gamma$  and  $B_s \rightarrow \gamma\gamma$ .

We have calculated the complete RPV one-loop contribution to these decays in the one-coupling scheme, i.e., assuming one contribution of a pair of RPV couplings at a time. We found that the RPV effect is dominated by a single one-loop diagram which was named  $\lambda$ -*irreducible*. This diagram has a distinct topology which is irrelevant to  $b \rightarrow s\gamma$  at one-loop. Therefore, since its effect on the one-photon decay  $B \rightarrow X_s\gamma$  is negligible at one-loop, the  $\lambda$ -*irreducible* RPV effects that were found for the two photons decays  $B_s \rightarrow X_s\gamma\gamma$  and  $B_s \rightarrow \gamma\gamma$  are uncorrelated to the decay  $B \rightarrow X_s\gamma$ .

We found that the  $\lambda$ -*irreducible* RPV diagram with a  $\tau$ -loop gives  $BR^{RPV}(B_s \rightarrow \gamma\gamma) \sim 16 \times BR^{SM}(B_s \rightarrow \gamma\gamma) \sim 5 \times 10^{-6}$ . In the case of  $B \rightarrow X_s\gamma\gamma$  the enhancement to the decay width is less dramatic:  $BR^{RPV}(B \rightarrow X_s\gamma\gamma) \sim 5 \times BR^{SM}(B \rightarrow X_s\gamma\gamma) \sim 6 \times 10^{-7}$ .

We have also shown that, in spite of the rather marginal RPV effect on the decay width of  $B \rightarrow X_s\gamma\gamma$ , other observables may be used to disentangle the  $\lambda$ -*irreducible* RPV contribution. In particular, we find that the energy distribution of the two photons is significantly different from the SM since it is sensitive to new threshold effects caused by the specific topology of the  $\lambda$ -*irreducible* diagram. Moreover, a forward-backward asymmetry with respect to the softer photon in  $B \rightarrow X_s\gamma\gamma$  is appreciably different from its SM value in the presence of the  $\lambda$ -*irreducible* RPV effect. Thus, these two observables may be used to provide an additional handle for discriminating different models, in particular RPV SUSY.

#### Acknowledgments

G.E. thanks the Technion President Fund for partial support.

- 
- [1] See e.g., H. E. Haber, G. L. Kane, Phys. Rep. **117**, 75 (1985); S.P.Martin, in **Perspectives on Supersymmetry** (edited by G.L.Kane), World Scientific, 1998, p.1.  
[2] G.-L. Lin, J. Liu and Y.-P. Yao, Phys. Rev. **D42**, 2314 (1990).  
[3] H. Simma and D. Wyler, Nucl. Phys. **B344**, 283 (1990).  
[4] S. Herrlich and J. Kalinowski, Nucl. Phys. **B381**, 501 (1992).  
[5] L. Reina, G. Ricciardi and A. Soni, Phys. Lett. **B396**, 231 (1997).  
[6] L. Reina, G. Ricciardi and A. Soni, Phys. Rev. **D56**, 5805 (1997).  
[7] S. Bertolini and J. Matias, Phys. Rev. **D57**, 4197 (1998).

- [8] J. Cao, Z. Xiao and G. Lu, Phys. Rev. **D64**, 014012 (2001).
- [9] W.-j. Huo, C. D. Lu and Z.-j. Xiao, hep-ph/0302177.
- [10] P. Singer and D.X. Zhang, Phys. Rev. **D56**, 4274 (1997); S.R. Choudhury, G.C. Joshi, Namit Mahajan and B.H.J. McKellar, Phys. Rev. **D67**, 074016 (2003).
- [11] K. Hagiwara *et al.*, Phys. Rev. **D66**, 010001 (2002).
- [12] A. Geminin, S. Bar-Shalom, G. Eilam and F. Krauss, Phys. Rev. **D67**, 115012 (2003). We take this opportunity to correct our results for  $\mu \rightarrow e\gamma\gamma$ : the rate has to be multiplied by a factor of 1/2.
- [13] H. Dreiner, in **Perspectives on Supersymmetry** (edited by G. L. Kane), World Scientific, 1998, p. 462.
- [14] B. C. Allanach, A. Dedes and H. K. Dreiner, Phys. Rev. **D60**, 075014 (1999).
- [15] G. Bhattacharyya, Nucl. Phys. Proc. Suppl. **52A**, 83 (1997).
- [16] R. Barbier *et al.*, hep-ph/9810232.
- [17] J.-H. Jang, Y.G. Kim and J.S. Lee, Phys. Rev. **D58**, 035006 (1998).
- [18] D.K. Ghosh, X-G. He, B.H.J. McKellar and J.-Q. Shi, JHEP **0207**, 067 (2002).
- [19] G. Bhattacharyya, D. Chang, C.-H. Chou and W.-Y. Keung, Phys. Lett. **B493**, 113 (2000).
- [20] S. Bar-Shalom, G. Eilam and Y.-D. Yang, Phys. Rev. **D67**, 014007 (2003).
- [21] R.M. Godbole, P. Roy and X. Tata, Nucl. Phys. **B401**, 67 (1993).
- [22] G. Bhattacharyya, J. Ellis and K. Sridhar, Mod. Phys. Lett. **A10**, 1583 (1995); G. Bhattacharyya, D. Choudhury and K. Sridhar, Phys. Lett. **B355**, 193 (1995); J. Ellis, S. Lola and K. Sridhar, **B408**, 252 (1997).
- [23] V. Barger, G. F. Giudice and T. Han, Phys. Rev. **D40**, 2987 (1989).